Rock Mech Rock Eng
DOI 10.1007/s00603-015-0754-6

TECHNICAL NOTE

Mechanical Analysis of Static Stress Within Fault-Pillars Based on a Voussoir Beam Structure

Zhen-lei Li[1] · Lin-ming Dou[1] · Wu Cai[1] · Gui-feng Wang[1] · Yan-lu Ding[1] · Yong Kong[1]

Received: 2 September 2014 / Accepted: 7 April 2015

Keywords Rock burst · Fault-pillar · Static stress · Voussoir beam structure

List of symbols

A, B, C	Rock blocks
A′, B′, C′	Action points of lateral thrust
H, L, W	Thickness, length and width of rock block (m)
h_0	Thickness-to-length ratio of rock block ($h_0 = H/L$)
L_x	Length of fault-pillar (m)
a	Thickness of voussoir arch (m)
δ_0, δ_1	Vertical deflections of rock blocks B and C (m)
α_A, α_B, α_C	Rotation angles of rock blocks A, B, and C (°)
θ	Angle of fault plane in vertical direction (°)
φ, φ_f	Friction angles of rock and fault plane (°), 0.85 for most rocks and faults
γ	Unit weight of rock (N/m^3), 2.5×10^4 N/m^3 for most rocks
p	Applied stress on rock block from overlying strata (Pa)
q	Total applied stress on rock block from overlying strata and the rock block ($q = p+\gamma H$) (Pa)
σ_c	Uniaxial compressive strength (UCS) of rock (Pa)
σ, τ	Compressive stress and shear stress at fault plane (Pa)
$f(l_x)$	Static stress within fault-pillar (Pa)
P	Total load on rock block ($P = pLW + \gamma HLW = qLW$) (N)
T	Lateral thrust (N)
R_{0-0}, R_{0-1}, R_{1-2}	Shear forces between rock blocks (N)
R, R_1	Resistance forces of collapsed and broken strata (N)
T_f, R_f	Normal force and shear force at fault plane (N)

1 Introduction

Rock bursts are currently considered to be one of the most severe threats to underground safety in coal mining. When mining activities approach faulted areas, rock bursts are more likely and thus often result in casualties. For instance, due to a fault, the extraction of longwall panel 25110 in the Yuejin coalmine suffered 20 rock bursts (Li et al. 2013). Therefore, rock bursts around faulted areas have been studied worldwide (Islam and Shinjo 2009; Ji et al. 2012; Li et al. 2011; Michalski 1977; Pan et al. 1998). The focus of these studies was the fault, while the fault-pillar (the coal pillar between the fault plane and the face line or gateway), has often been overlooked. The concept of fault-

✉ Lin-ming Dou
lmdou@cumt.edu.cn; kdlzl2010@163.com

Zhen-lei Li
cumtzhenleili@163.com

[1] State Key Laboratory of Coal Resources and Safe Mining, China University of Mining and Technology, Xuzhou 221116, Jiangsu, China

Published online: 17 April 2015

pillar induced rock bursts (FPIRB) was first proposed and analysed by Li et al. (2013, 2014) who investigated the mechanisms underpinning FPIRB behaviour and calculated the static stress within the fault-pillar through a fault-pillar model, which proved that high static stress within the fault-pillar is a key factor inducing rock bursts. Unfortunately, the voussoir beam structure in their model was based on Qian (1982). Thus, the arch compression thickness and buckling failure of the voussoir beam were neglected. Also, the lateral thrust and shear forces were only approximate. As a result, the accuracy of the static stress calculated through their model is poor.

This research is aimed at improving the fault-pillar model to investigate the static stress within the fault-pillar in a more precise way, and analyse which parameter influences the static stress most from a theoretical viewpoint. To this end, the voussoir beam structure developed by Qian et al. (1994a) is used and an enhanced fault-pillar model is proposed considering the voussoir arch thickness. Although Qian et al. (1994a) deduced a more reasonable lateral thrust and shear forces, they only obtained limiting conditions against sliding failure and crushing failure. Hence, before analysis of the fault-pillar model, the limiting condition against buckling failure is firstly deduced.

2 Background

The voussoir beam analogue was first proposed by Evans (1941). Subsequently Beer and Meek (1982), Sofianos (1996), Diederichs and Kaiser (1999), Brady and Brown (2004) published seminal work on this problem (Fig. 1a). More recently, the voussoir beam was still studied by scholars, like Talesnick et al. (2007); Tsesarsky (2012). In China, Qian (Chien 1981; Qian 1981, 1982) proposed a voussoir beam structure specific to longwall mining based on the investigation of the subsidence of overlying strata at longwall working areas (Fig. 1b, c). This kind of structure was visualised by Ju and Xu (2013) through a physical simulation. Limiting conditions, shear forces, and lateral thrust in the structure were general at best since the voussoir arch thickness was neglected and the rotation angle of adjacent blocks was assumed equal. Subsequently Qian et al. (1994a) considered the voussoir arch thickness and did a reasonable analysis of key blocks in the structure so that these problems were solved (Fig. 2). The structure was applied to field practice and verified and validated (Qian et al. 1994b; Cao et al. 1998).

According to Qian et al. (1994a), the voussoir arch thickness, lateral thrust, and shear forces are given by:

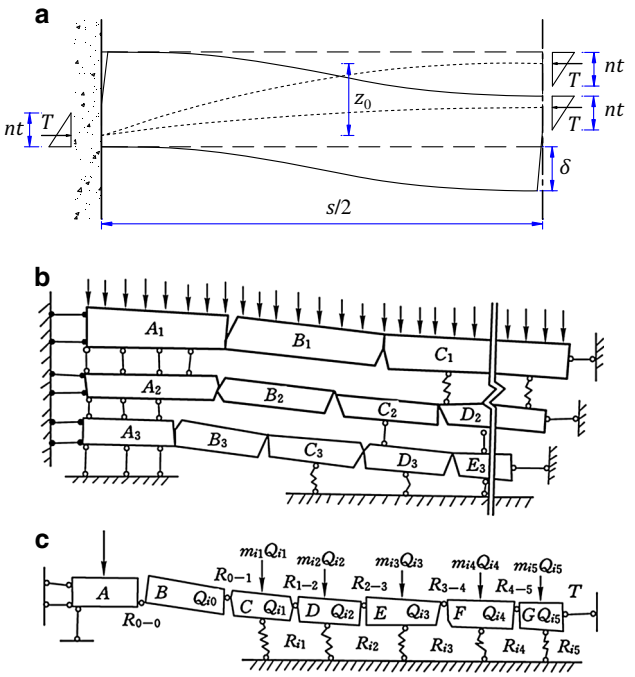

Fig. 1 Voussoir beam models by **a** Sofianos (1996) and **b**, **c** Qian (1981). **b** Complete voussoir beam structure demonstrating movement and behaviour of overlying strata after longwall mining, **c** voussoir beam structure for a certain roof bed

$$\begin{cases} a = \dfrac{1}{2}(H - L \cdot \sin\alpha_B) \\ T = \dfrac{2}{2h_0 - \sin\alpha_B} \cdot q \cdot L \\ R_{0-0} = \dfrac{4h_0 - 3\sin\alpha_B}{2(2h_0 - \sin\alpha_B)} \cdot q \cdot L \\ R_{0-1} = R_{1-2} = \dfrac{\sin\alpha_B}{2(2h_0 - \sin\alpha_B)} \cdot q \cdot L \end{cases} . \quad (1)$$

Limiting conditions against sliding failure and crushing failure are given by:

$$\mathrm{F.S.}_{\mathrm{slide}}(h_0, \alpha_B) = \frac{3}{4}\sin\alpha_B - h_0 + \tan\phi \geq 0, \quad (2)$$

$$\mathrm{F.S.}_{\mathrm{crush}}(h_0, \alpha_B) = \frac{1}{4}\eta \cdot (\sin^2\alpha_B - 3h_0 \cdot \sin\alpha_B + 2h_0^2) - \frac{q}{\sigma_c} \geq 0, \quad (3)$$

where η is the squeezing coefficient of the block abutment. η, which is obtained experimentally, is defined as the ratio of the squeezing strength of the block abutment to the UCS of the rock block. The squeezing strength is the strength when the block abutment is stressed by normal compressive stress and shear stress simultaneously.

Buckling failure will occur when the critical deflection of block B is exceeded. To avoid buckling failure, the voussoir arch thickness and the moment arm $(H - \delta_1 - a)$

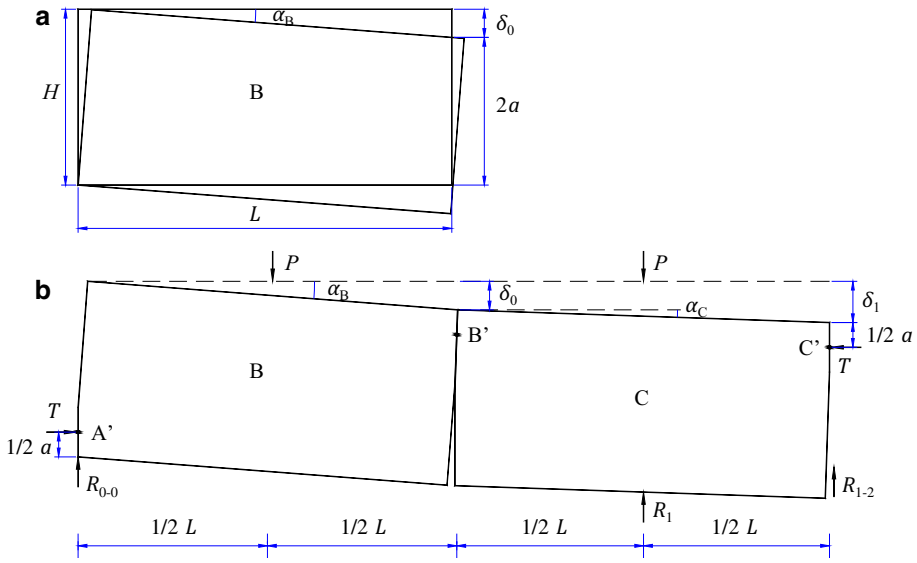

Fig. 2 Model of key blocks B and C in the voussoir beam structure (Qian et al. 1994a). **a** Geometric disposition when rock blocks rotate, **b** displaced state of, and stresses on, key blocks

(Fig. 2) of the reaction force (T) must be positive values. Necessary conditions are:

$$\begin{cases} a = \dfrac{1}{2}(H - L \cdot \sin\alpha_B) > 0 \\ (H - \delta_1 - a) > 0 \end{cases}. \tag{4}$$

According to Qian et al. (1994a), the deflections of blocks B and C are given by:

$$\delta_0 = L \cdot \sin\alpha_B,\ \delta_1 = \frac{5}{4} L \cdot \sin\alpha_B. \tag{5}$$

Substituting Eq. (5) into Eq. (4), the criterion against buckling failure is given by:

$$\text{F.S.}_{\text{buckle}}(h_0, \alpha_B) = -\frac{3}{2}\sin\alpha_B + h_0 > 0. \tag{6}$$

Note Eqs. (2), (3), and (6) are used to judge whether the voussoir beam structure is stable so as to determine which fault-pillar model to apply in Sect. 3. Equation (1) is used to calculate the lateral thrust and shear forces that are used in the fault-pillar model.

It is well known that for normal stresses of up to 200 MPa the coefficient of friction is approximately 0.85 for most rocks and faults (Byerlee 1978). Through squeezing experiments on rock blocks, Huang et al. (2000) concluded that the squeezing coefficient might be 0.36–0.42 (0.4 on average). Hence, tanφ and η are set to 0.85 and 0.4, respectively. Limiting cases for beam stability are illustrated in Fig. 3. It is seen that there is a maximum load (q) the beam allows for certain h_0 and α_B and that beams with larger deflections are more likely to fail.

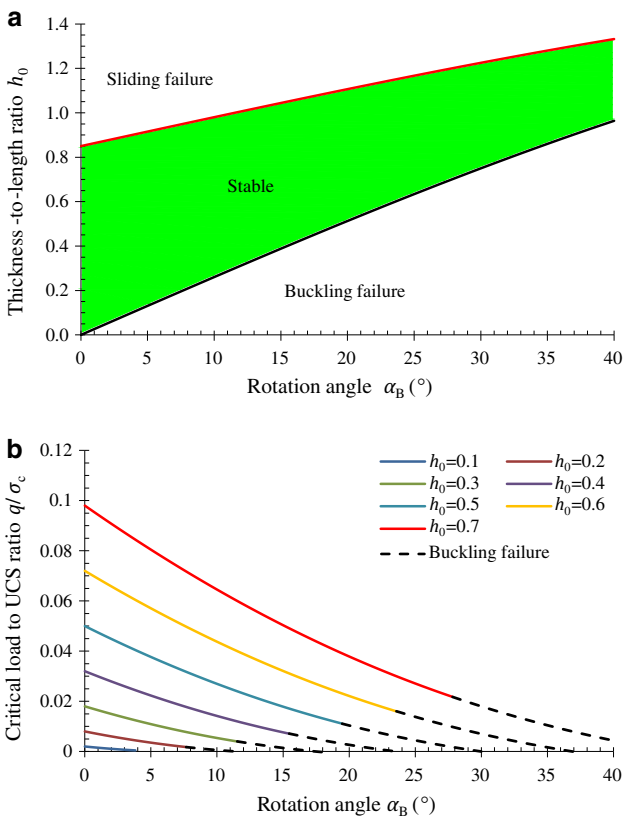

Fig. 3 Limiting cases for beam stability: **a** critical limits against sliding failure [the *red solid line*, corresponds to Eq. (2)] and buckling failure [the *black solid line* corresponds to Eq. (6)], **b** critical limits against crushing failure. In **b**, the *lines* are calculated by using Eq. (3). Note that tanφ [in Eq. (2)] and η [in Eq. (3)] are set to 0.85 and 0.4

3 Mechanical Analysis of a Fault-Pillar

Consider a normal case of FPIRB, as shown in Fig. 4: the longwall face advances from right to left. The fault-pillar, located between the face line and the geological fault, bears a high static stress. The presence of a hard/thick stratum is assumed in the simplified form of a beam to establish the fault-pillar model. The occurrence of such a stratum is quite common (Xuan et al. 2014). Since the hard/thick stratum may, or may not, form a voussoir beam structure, there are two cases tested in the model. Either the voussoir beam structure is formed and maintained, or it is absent (Fig. 5). In both cases, block A will inevitably rotate when the pillar length is reduced to a certain value.

3.1 A Voussoir Beam Structure is Present (P.)

In brief, this case is referred to as 'P.': before rotation of block A (referred to as 'B.R.') (Fig. 5a), a compression arch develops within block B, rising from the left to the right. There is compressive stress and shear stress on the fault plane and a lateral thrust and shear force at the right-hand side of block A. At the top and bottom of block A, there is a distributed load from the overlying strata and a resistance stress from the fault-pillar. After rotation of block A (referred to as 'A.R.') (Fig. 5b), a compression arch develops within block A, rising from the abutment at the fault plane to the high point at the right side of block A. For the sake of simplicity, the compressive stress (σ), shear stress (τ), and distributed load (p) are assumed to have been uniformly distributed.

Block A will slide at the fault plane and rotate when the actual shear stress exceeds the maximum shear stress permitted on the fault plane. Hence, the criterion against rotation of block A (referred to as 'rotation criterion') is given by:

$$\mathrm{F.S.}_{\text{rotation}-\mathrm{P.}} = \sigma \cdot \tan\phi_f - \tau \geq 0. \tag{7}$$

Mechanical equilibrium of block A requires, before rotation

$$\begin{cases} \sigma \cdot H - \tau \cdot H \cdot \tan\theta - T = 0 \\ \int_0^{L_x} f(l_x)\mathrm{d}l_x - \tau \cdot H - R_{0-0} - \sigma \cdot H \cdot \tan\theta - p \cdot (L - H \cdot \tan\theta) - \gamma \cdot H \cdot \left(L - \frac{1}{2}H \cdot \tan\theta\right) = 0 \\ \int_0^{L_x} f(l_x) \cdot l_x \mathrm{d}l_x + \frac{1}{2}T \cdot a - R_{0-0} \cdot L - \frac{\sigma \cdot H^2}{2\cos^2\theta} - \frac{1}{3}\gamma \cdot H^3 \cdot \tan^2\theta \\ \quad -\frac{1}{2}(p + \gamma \cdot H) \cdot (L^2 - H^2 \cdot \tan^2\theta) = 0 \end{cases}. \tag{8}$$

and after rotation

$$\begin{cases} T_f \cdot \cos\theta + R_f \cdot \sin\theta - T = 0 \\ \int_0^{L_x} f(l_x)dl_x + R_f \cdot \cos\theta + R_{0-1} - T_f \cdot \sin\theta \\ \quad - p \cdot (L - H \cdot \tan\theta) - \gamma \cdot H \cdot \left(L - \frac{1}{2}H \cdot \tan\theta\right) = 0 \\ \int_0^{L_x} f(l_x) \cdot l_x dl_x + T \cdot \left(H - \delta_0 - \frac{1}{2}a\right) + R_{0-1} \cdot L \\ \quad - T_f \cdot a \cdot \frac{1}{2\cos\theta} - \frac{1}{3}\gamma \cdot H^3 \cdot \tan^2\theta \\ \quad -\frac{1}{2}(p + \gamma \cdot H) \cdot (L^2 - H^2 \cdot \tan^2\theta) = 0. \end{cases} \tag{9}$$

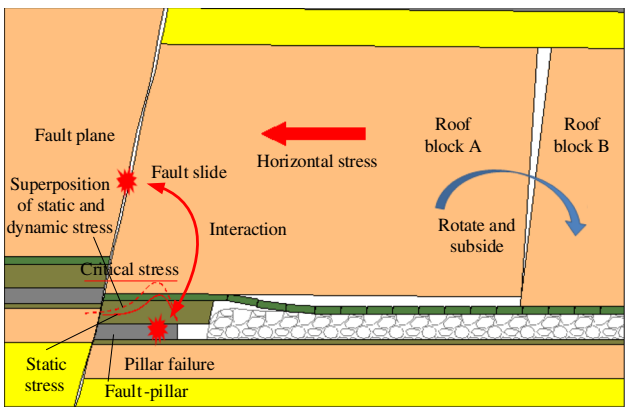

Fig. 4 Sketch of the FPIRB mechanism (Li et al. 2014)

3.2 A Voussoir Beam Structure is Absent (A.)

This case is briefly referred to as 'A.'. In case A., block B has collapsed. Thus, there is no force in effect between blocks A and B. The problem may be analysed in terms of the problem geometry illustrated in Fig. 5c, d. Before rotation, the pillar itself bears load. However, after rotation, the pillar, together with the collapsed and broken strata, supports the load.

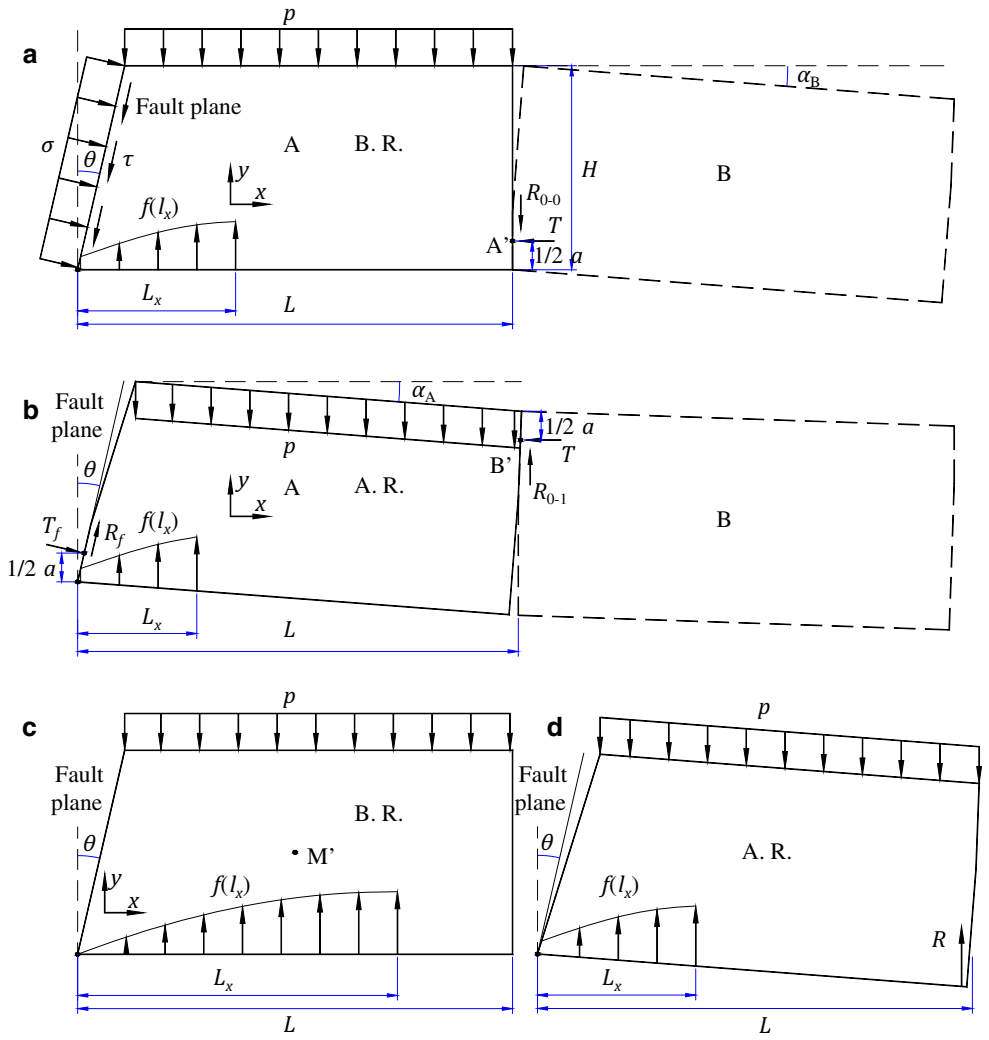

Fig. 5 Fault-pillar model: **a** and **b** a voussoir beam structure is present, **c** and **d** a voussoir beam structure is absent. B.R. is before rotation of block A, A.R. is after rotation of block A

The equilibrium in Fig. 5c requires that the action points of the load and $f(l_x)$ in the y-coordinate are the same (maybe at point M′), which indicates that the stress distribution, $f(l_x)$, within the pillar was variable when the pillar length decreases. Thus, the problem concerning the distribution of $f(l_x)$ is fundamentally indeterminate and the exact rotation criterion is difficult to obtain. In the extreme case, block A rotates when the pillar length is less than one half of the block length. The rotation criterion is given by:

$$\text{F.S.}_{\text{rotation}-A.} = L_x - \frac{1}{2}L > 0. \tag{10}$$

Mechanical equilibrium of block A requires, before rotation:

$$\int_0^{L_x} f(l_x)dl_x - p \cdot (L - H \cdot \tan\theta) - \gamma \cdot H \cdot \left(L - \frac{1}{2}H \cdot \tan\theta\right) = 0 \tag{11}$$

and after rotation:

$$\begin{cases} \int_0^{L_x} f(l_x)dl_x + R - p \cdot (L - H \cdot \tan\theta) \\ \quad -\gamma \cdot H \cdot \left(L - \frac{1}{2}H \cdot \tan\theta\right) = 0 \\ \int_0^{L_x} f(l_x) \cdot l_x dl_x + R \cdot L - \frac{1}{3}\gamma \cdot H^3 \cdot \tan^2\theta \\ \quad -\frac{1}{2}(p + \gamma \cdot H) \cdot (L^2 - H^2 \cdot \tan^2\theta) = 0 \end{cases}. \tag{12}$$

3.3 Guidelines on the Use of Equations

Figure 6 shows the process required to handle the problem of interest here. First, we obtain the relevant parameters: then, we judge whether, or not, a stable voussoir beam structure is present by using Eqs. (2), (3), and (6). When

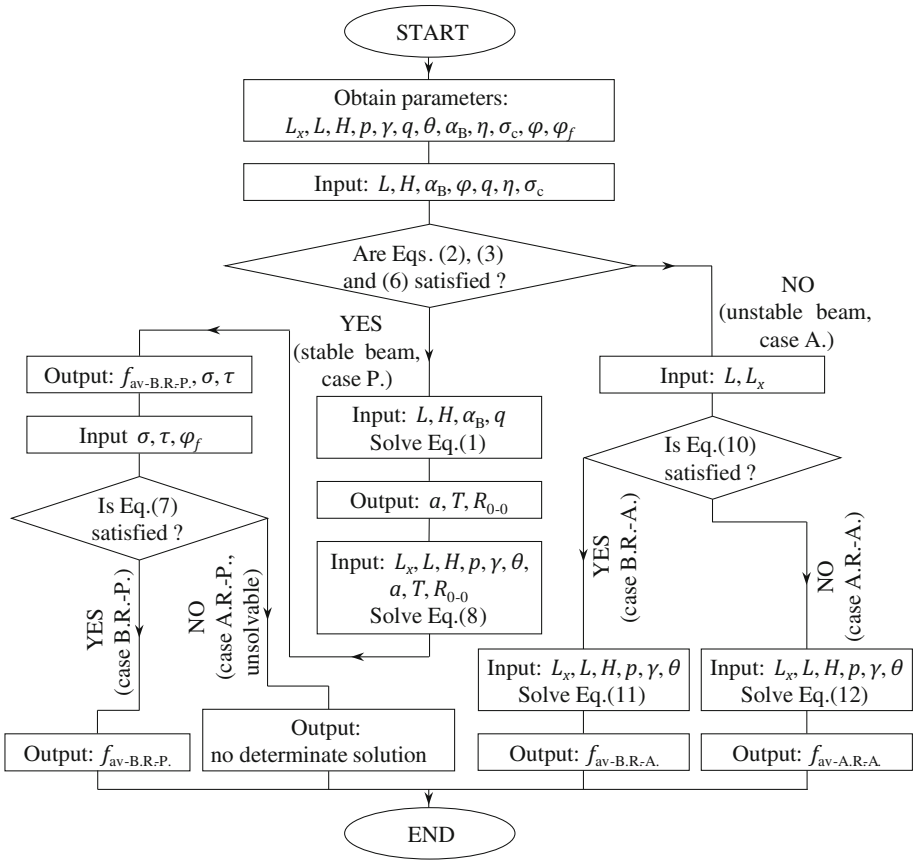

Fig. 6 Flowchart for the calculation of static stress within the fault-pillar. P. is the case when a voussoir beam structure is present, A. is the case when a voussoir beam structure is absent, B.R. is before rotation of block A, A.R. is after rotation of block A

each of the equations is satisfied, case P. is used. Otherwise, case A. is used. In case A., we judge whether block A rotates by using Eq. (10). If not, choose Eq. (11) to calculate the static stress ($f_{\text{av-B.R.-A.}}$). Otherwise, introduce parameters in Eq. (12) and output the static stress ($f_{\text{av-A.R.-A.}}$). In case P., we firstly introduce parameters to Eq. (1) to obtain a, T, and $R_{0\text{–}0}$. Then we introduce a, T, $R_{0\text{–}0}$, and other relevant parameters in Eq. (8) to obtain $f_{\text{av-B.R.-P.}}$, σ, and τ. Then we introduce σ, τ, and φ_f in Eq. (7) to judge whether, or not, block A rotates. If not, output the static stress ($f_{\text{av-B.R.-P.}}$). Otherwise, there is no determinate solution to the problem.

4 Discussion

According to the fault-pillar model, the static stress within the pillar is divided into four terms and calculated by Eqs. (8), (9), (11), and (12), respectively. Note that each of the four equations corresponds to a certain condition. In theory, if the actual static stress distribution and related parameters are determined, the static stress can be calculated and used to evaluate rock burst risk according to the derivation process of the model. However, not all of the equations have determinate solutions.

For a specific longwall panel, parameters L, L_x, H, θ, p, and γ are obtained by physical measurement. Therefore, when the distribution, $f(l_x)$, is confirmed or assumed, the static stress in case A. can be solved by Eqs. (11) and (12). In Fig. 5a or b, the lateral thrust and shear forces can (or cannot) be calculated by Eq. (1) because the stress state of the compression arch in Fig. 5a or b is the same as (or different from) that in Fig. 2b. Hence, in case P. $f(l_x)$ can be solved by Eq. (8) while there is no determinate solution to Eq. (9), which is because there are five unknown variables [T_f, R_f, $f(l_x)$, T, $R_{0\text{–}1}$] in Eq. (9). In summary, there are solutions to Eqs. (8), (11), and (12), but not to Eq. (9).

To solve engineering problems, $f(l_x)$ is assumed to follow a triangular load distribution which is the basis of the subsequent discussion. This allows derivation of an average static stress, f_{av}, in the fault-pillar. A correction coefficient, K, is defined so that the actual average static stress is Kf_{av}. K is obtainable from a combination of theoretical calculation and in situ pressure measurement. As an example, the solution to Eq. (8) is given by:

$$\begin{cases} f_{\mathrm{av}} = \dfrac{1}{2L_x \cdot (4L_x - 3H \cdot \tan\theta)} \cdot [6R_{0-0} \cdot (2L - H \cdot \tan\theta) + 6T \cdot (H - a) \\ \quad +6q \cdot L \cdot (L - H \cdot \tan\theta) + \gamma \cdot H^3 \cdot \tan^2\theta] \\ \sigma = \dfrac{\cos^2\theta}{H \cdot (4L_x - 3H \cdot \tan\theta)} \cdot [2R_{0-0} \cdot (3L - 2L_x) \cdot \tan\theta + T \cdot (4L_x - 3a \cdot \tan\theta) \\ \quad +q \cdot \tan\theta \cdot (L - H \cdot \tan\theta) \cdot (3L - 4L_x + 3H \cdot \tan\theta) - 2\gamma \cdot H^2 \cdot \tan^2\theta \cdot (L_x - H \cdot \tan\theta)] \\ \tau = \dfrac{\cos\theta}{H \cdot (4L_x - 3H \cdot \tan\theta)} \cdot [2R_{0-0} \cdot (3L - 2L_x) + T \cdot (3\dfrac{H}{\cos^2\theta} - 3a - 4L_x \cdot \tan\theta) \\ \quad +q \cdot (L - H \cdot \tan\theta) \cdot (3L - 4L_x + 3H \cdot \tan\theta) - 2\gamma \cdot H^2 \cdot \tan\theta \cdot (L_x - H \cdot \tan\theta)] \end{cases} \tag{13}$$

Parameters influencing the static stress include L_x, L, H, q, α_B, θ, and h_0 (where $h_0 = H/L$). In the subsequent paragraphs, the influence of these parameters on the static stress is discussed. For simplicity, the fault angle is assumed to be zero ($\theta = 0$).

By combining Eqs. (1) and (5) with Eqs. (8), (11), and (12), the average static stress and rotation criterion are given by:

$$\begin{cases} f_{\mathrm{av-B.R.-P.}} = \dfrac{3(7h_0 - 3\sin\alpha_B)}{4(2h_0 - \sin\alpha_B)} \cdot q \cdot \dfrac{L^2}{L_x^2} \\ f_{\mathrm{av-B.R.-A.}} = q \cdot \dfrac{L}{L_x} \\ f_{\mathrm{av-A.R.-A.}} = q \cdot \dfrac{3L^2}{2(3L - 2L_x) \cdot L_x} \end{cases} . \tag{14}$$

$$\begin{cases} \mathrm{F.S.}_{\mathrm{rotation-P.}} = -\dfrac{3}{8}(7h_0 - 3\sin\alpha_B) \cdot \dfrac{L}{L_x} \\ \quad + \dfrac{1}{4}(8h_0 - 5\sin\alpha_B) + \tan\phi_f \geq 0 \\ \mathrm{F.S.}_{\mathrm{rotation-A.}} = L_x - \dfrac{1}{2}L > 0 \end{cases} \tag{15}$$

It may be seen that the rotation criterion and the formulae for static stress in case A. are simpler. Thus, case P. became our focus. Figure 7 shows some examples illustrating the variation of static stress as obtained through Eq. (14). In all cases, for the same L_x, the stresses in cases with a larger value of L are higher. In case A., the stresses are much lower. In case B.R.-P., stresses rise to maximum values immediately before rotation. The maximum values differ greatly for different α_B and h_0, whereas they are equal for the same α_B and h_0 even if L were different, which is because the values of α_B and h_0 determine the critical ratio L/L_x that determines the rotation of block A, as shown in Fig. 8. Figure 8 indicates that thick beams, under small deflection, tend to rotate and the critical value of L/L_x increases rapidly when α_B rises to an extent almost sufficient to induce buckling failure. Overall, the critical L/L_x value differs greatly for different α_B and h_0, which is the root cause of the difference in the maximum value of $f_{\mathrm{av-B.R.-P.}}$. The coefficient $[3(7h_0 - 3\sin\alpha_B)]/[4(2h_0 - \sin\alpha_B)]$ in $f_{\mathrm{av-B.R.-P.}}$ varies from 2.625 to 2.8125 within various ranges of α_B and h_0, which implies that this coefficient has a limited influence on the static stress.

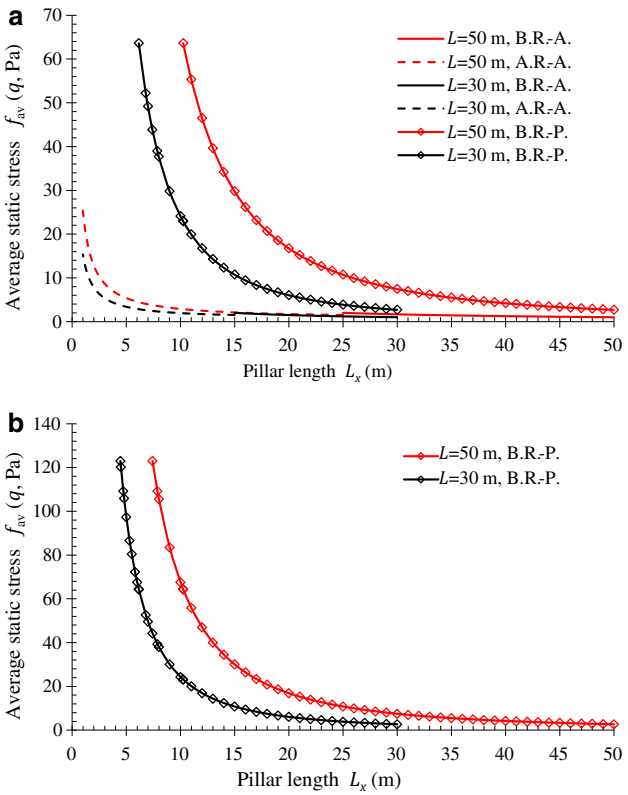

Fig. 7 Variation of the average static stress versus pillar length. **a** $h_0 = 0.7$, $\alpha_B = 10°$; **b** $h_0 = 0.5$, $\alpha_B = 10°$. Note that the ordinate is in multiples of the total applied stress, q, in 'Pa'. Data are calculated by using Eq. (14) and the rotation of block A is based on Eq. (15) (i.e. the rotation criterion), and $\tan\varphi_f$ is set to 0.85

In case A.R.-P., $f(l_x)$ cannot be deduced from the use of Eq. (9), as discussed above. By comparing Fig. 5b with Fig. 5d, it is concluded that $f_{\mathrm{av-A.R.-P.}}$ is less than $f_{\mathrm{av-A.R.-A.}}$ (i.e. $f_{\mathrm{av-A.R.-P.}} < q \cdot \frac{3L^2}{2(3L-2L_x)\cdot L_x}$), which implies that the stress in case P. drops significantly upon rotation.

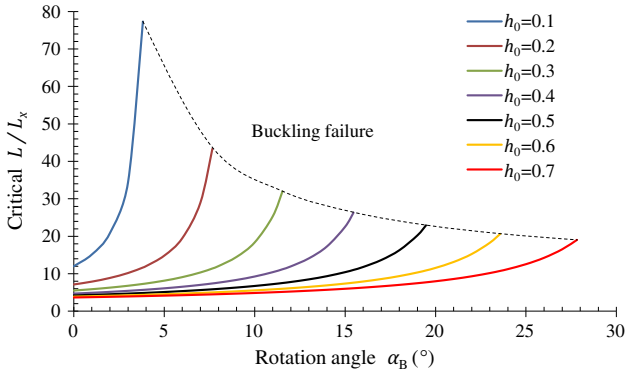

Fig. 8 Variation of the critical block length-to-pillar length ratio versus rotation angle and thickness-to-length ratio against rotation of block A. Values greater than this imply some rotation of block A. Data are calculated by using Eq. (15), and $\tan\varphi_f$ is set to 0.85

In cases A. and P., the stress after rotation is normally lower than the maximum stress in case B.R.-P.. For example, in Fig. 7a the maximum value of $f_{\text{av-B.R.-P.}}$ exceeds $63q$, while $f_{\text{av-A.R.-A.}}$ is lower than $16q$ and $26q$ when the pillar length decreases to 1 m. Actually, within various ranges of α_B and h_0, the critical ratio L/L_x all exceeds 3.5 [see Eq. (15) and Fig. 8] when $\tan\varphi_f = 0.85$, which implies that the maximum values of $f_{\text{av-B.R.-P.}}$ exceed $32q$ immediately before rotation of block A [see Eq. (14)] among various values of α_B, h_0, L, and L_x.

From Eq. (3) and Fig. 3b, it may be seen that there is a limited q for a stable voussoir beam structure. For instance, maximum values of q are 0.0645 and 0.0270 σ_c in cases where $h_0 = 0.7$, $\alpha_B = 10°$ and $h_0 = 0.5$, $\alpha_B = 10°$. Therefore, the maximum values of $f_{\text{av-B.R.-P.}}$ in Fig. 7a, b reach approximately 4.11 and 3.32 σ_c, respectively. Under such high stresses, a pillar normally fails. Note that the aforementioned values are for the critical case when a stable voussoir beam structure is on the verge of crushing failure and the rotation of block A is imminent. Actual values may be far lower.

Through this discussion, it is seen that stresses in case B.R.-P. are the highest. Maximum values occur when a stable voussoir beam structure is on the verge of crushing failure and the rotation of block A is imminent. The values of α_B and h_0 have the most influence on the maximum stress values, and the maximum stress values are smaller in cases with a smaller value of α_B and a larger value of h_0.

5 Conclusions

The fault-pillar model is a simplification of in situ mining-geological conditions and contains many parameters. Some of the parameters are difficult to obtain, or are not constant, because of the complicated mining-geological conditions. For example, the values can be investigated for the lengths of blocks B and C in the voussoir beam structure but not the length of the block next to the fault (i.e. block A). Also, the thickness of the roof bed varies significantly, even for the same longwall panel. In addition, it is almost impossible to realise in situ conditions that are exactly the same as those modelled. All of these factors prevent the use of the model to calculate the static stress within the pillar with precision. What is important is the estimation of the variation of static stress and its main influencing parameters. If possible, influencing parameters should be pre-controlled to reduce the static stress as far as is possible so that rock burst risk is concomitantly reduced.

The stress state within the fault-pillar fits one of four cases: a voussoir beam structure is present and before/after rotation of block A (B.R.-P./A.R.-P.), a voussoir beam structure is absent and before/after rotation of block A (B.R.-A./A.R.-A.). The stress in case B.R.-P. is much higher than in the other cases. In all cases, the stress shows a positive correlation with L/L_x. In case A., the stress is affected by L and L_x. In case P., the influencing parameters are α_B, h_0, L, and L_x, among which α_B and h_0 show the most influence. The maximum stress values are smaller in cases with a smaller value of α_B and a larger value of h_0.

Acknowledgments This work was supported and financed by the Research and Innovation Project for College Graduates of Jiangsu Province (No. CXZZ12_0949), the National Natural Science Foundation of China and the Shenhua Group Corporation Limited (No. 51174285), and the Priority Academic Program Development of Jiangsu Higher Education Institutions (No. SZBF2011-6-B35).

References

Beer G, Meek JL (1982) Design curves for roofs and hanging-walls in bedded rock based on 'voussoir' beam and plate solutions. Trans Inst Min Metall 91:A18–A22

Brady BHG, Brown ET (2004) Rock mechanics for underground mining, 3rd edn. Kluwer Academic Publisher, Dordrecht

Byerlee JD (1978) Friction of rocks. Pure appl Geophys 116(4–5):615–626

Cao SG, Miao XX, Qian MG (1998) Stability and application of bond-beam structure. Coal Technol Northeast China (5):21–25 (in Chinese)

Chien MG (1981) A study of the behaviour of overlying strata in longwall mining and its application to strata control. Dev Geotech Eng 32:13–17. doi:10.1016/B978-0-444-42086-2.50008-9

Diederichs MS, Kaiser PK (1999) Stability of large excavations in laminated hard rock masses: the voussoir analogue revisited. Int J Rock Mech Min Sci 36(1):97–117

Evans WH (1941) The strength of undermined strata. Trans Inst Min Metall 50:475–500

Huang QX, Shi PW, Qian MG (2000) Experiment study on the coefficients of friction and inserting of main roof block corner. Rock Soil Mech 21(1):60–63 (in Chinese)

Islam MR, Shinjo R (2009) Mining-induced fault reactivation associated with the main conveyor belt roadway and safety of

the Barapukuria Coal Mine in Bangladesh: constraints from BEM simulations. Int J Coal Geol 79(4):115–130

Ji HG, Ma HS, Wang JA, Zhang YH, Cao H (2012) Mining disturbance effect and mining arrangements analysis of near-fault mining in high tectonic stress region. Safety Sci 50(4):649–654

Ju JF, Xu JL (2013) Structural characteristics of key strata and strata behaviour of a fully mechanized longwall face with 7.0 m height chocks. Int J Rock Mech Min Sci 58:46–54

Li ZH, Dou LM, Cao AY, Fan J, Mu ZL (2011) Mechanism of fault slip induced rockburst during mining. J China Coal Soc 36(S1):68–73 (in Chinese)

Li ZL, Dou LM, Cai W, He J, Wang GF, Liu J, Han RJ (2013) Fault-pillar induced rock burst mechanism of thick coal seam in deep mining. Chin J Rock Mech Eng 32(2):333–342 (in Chinese)

Li ZL, Dou LM, Cai W, Wang GF, He J, Gong SY, Ding YL (2014) Investigation and analysis of the rock burst mechanism induced within fault-pillars. Int J Rock Mech Min Sci 70:192–200

Michalski A (1977) Assessment of rock burst hazard in the approach of a caved longwall to a fault. Przeglad Gorniczy 23(9):387–397 (in Polish)

Pan YS, Wang LG, Zhang MT, Xu BY (1998) The theoretical and testing study of fault rockburst. Chin J Rock Mech Eng 17(6):642–649 (in Chinese)

Qian MG (1981) Conditions required for equilibrium of overlying strata at working areas. J China Inst Min Technol (2):31–40 (in Chinese)

Qian MG (1982) A structural model of overlying strata in longwall working and its application. J China Inst Min Technol (2):1–11 (in Chinese)

Qian MG, Miao XX, He FL (1994a) Analysis of key block in the structure of voussoir beam in longwall mining. J China Coal Soc 19(6):557–563 (in Chinese)

Qian MG, Zhang DL, Li LJ, Kang LX, Xu JL (1994b) "S-R" stability for the voussoir beam and its application. Ground Press Strata Control (3):6–11 (in Chinese)

Sofianos AI (1996) Analysis and design of an underground hard rock voussoir beam roof. Int J Rock Mech Min Sci Geomech Abstr 33(2):153–166

Talesnick ML, Ya'acov NB, Cruitoro A (2007) Modeling of a multiply jointed voussoir beam in the centrifuge. Rock Mech Rock Eng 40(4):383–404

Tsesarsky M (2012) Deformation mechanisms and stability analysis of undermined sedimentary rocks in the shallow subsurface. Eng Geol 133–134:16–29

Xuan DY, Xu JL, Zhu WB (2014) Dynamic disaster control under a massive igneous sill by grouting from surface boreholes. Int J Rock Mech Min Sci 71:176–187